Stabilization of cubic Sr_2FeMoO_6 through topochemical reduction

Daniel D. Taylor[a], Nathaniel J. Schreiber[a], Craig M. Brown[b,c], Angel M. Arevalo-Lopez[d], and Efrain E. Rodriguez[a,e]

[a] Department of Materials Science and Engineering, University of Maryland, College Park, Maryland, 20742-2115, USA

[b] NIST Center for Neutron Research, National Institute of Standards and Technology, Gaithersburg, Maryland 20899, USA.

[c] Department of Chemical and Biomolecular Engineering, University of Delaware, Newark, Delaware 19716, USA

[d] Centre for Science at Extreme Conditions, The University of Edinburgh, Edinburgh, EH9 3FD, UK

[e] Department of Chemistry & Biochemistry, University of Maryland, College Park, Maryland, 20742-4454, USA. E-mail: efrain@umd.edu

Electronic Supplemental Information

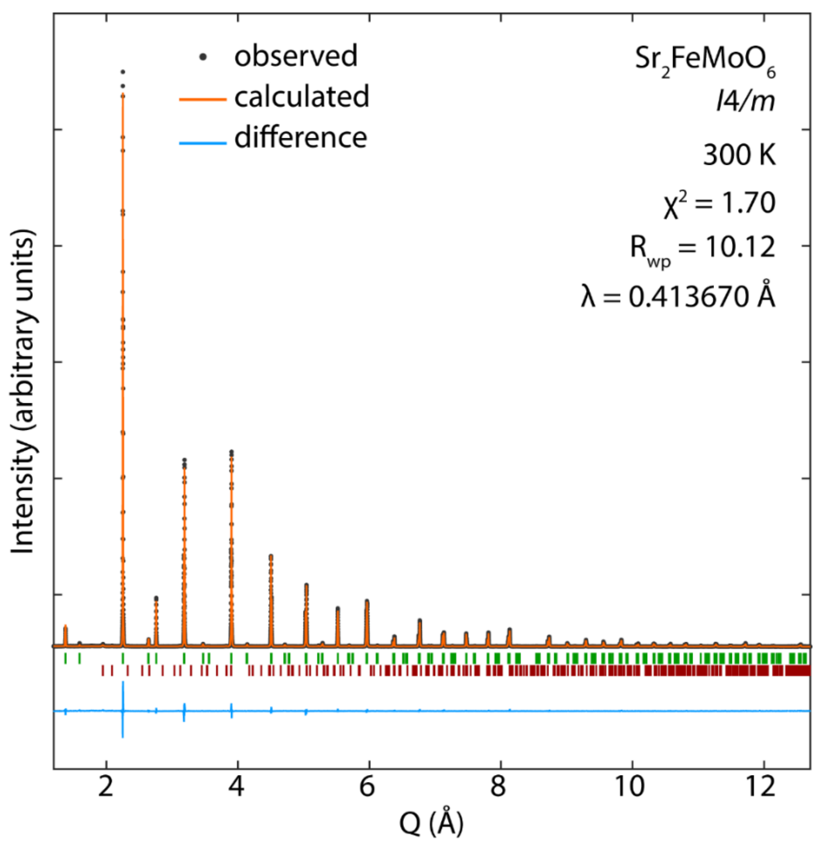

Figure S1. Synchrotron X-ray powder diffraction data of starting material, Sr_2FeMoO_6, collected at 300 K. The locations of the allowed reflections for Sr_2FeMoO_6 are shown as green tick marks, and the locations of allowed reflections for $SrMoO_4$ are shown as red tick marks, below the observed and calculated patterns. The presence of $SrMoO_4$ was only detected in Synchrotron XRD experiments. Neutron powder diffraction, a truly bulk technique, showed the sample to be pure Sr_2FeMoO_6.

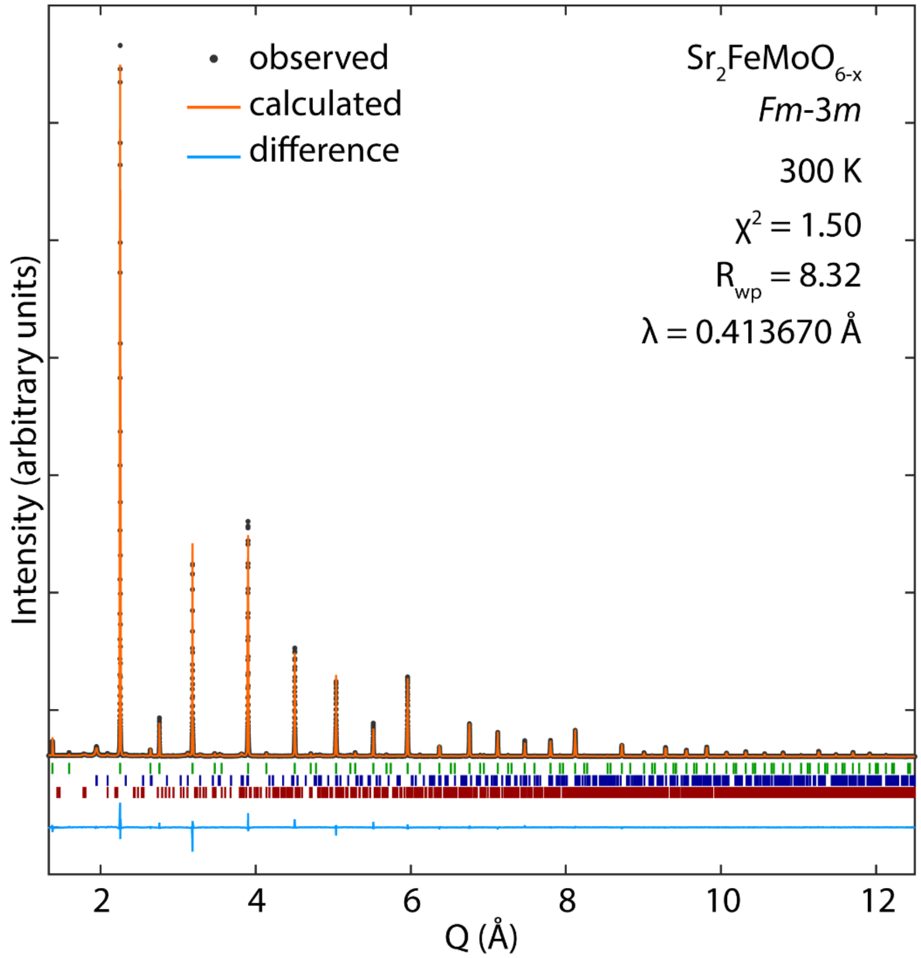

Figure S2. Synchrotron X-ray powder diffraction data of reduced material, Sr_2FeMoO_{6-x}, collected at 300 K. The locations of the allowed reflections for Sr_2FeMoO_{6-x} are shown as green tick marks, the locations of allowed reflections for $SrMoO_4$ are shown as blue tick marks, and the locations of allowed reflections for $SrCO_3$ are shown as red tick marks, below the observed and calculated patterns. The presence of $SrMoO_4$ and $SrCO_3$ were only detected in Synchrotron XRD experiments. Neutron powder diffraction, a truly bulk technique, showed the sample to be pure Sr_2FeMoO_{6-x}.

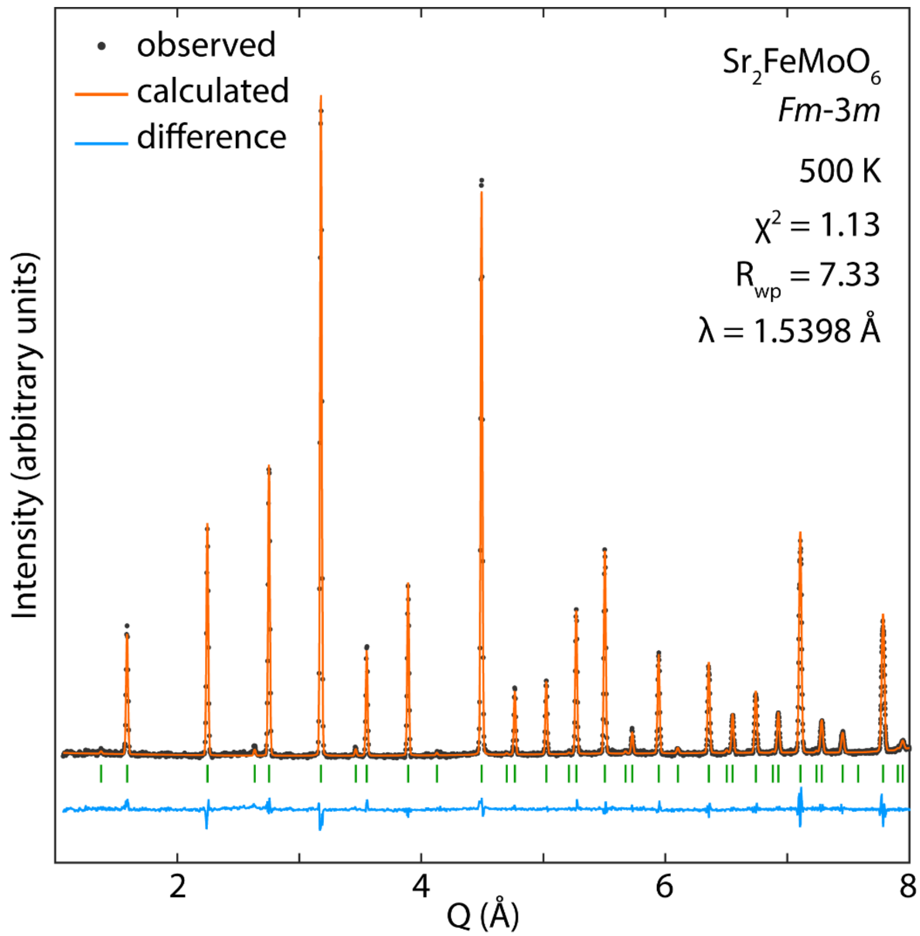

Figure S3. Neutron powder diffraction data of starting material, Sr_2FeMoO_6, collected at 500 K. The locations of the allowed reflections for Sr_2FeMoO_6 are shown as green tick marks below the observed and calculated patterns.

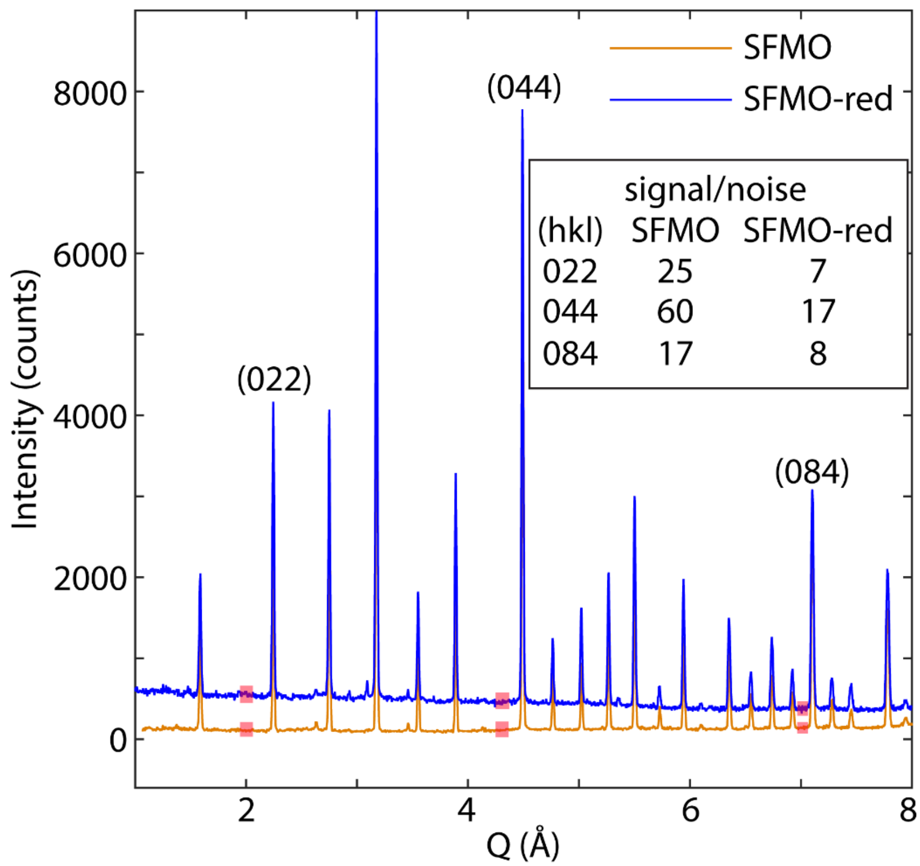

Figure S4. Overlay of the NPD patterns collected at 500 K. The background for the reduced sample (SFMO-red) is large and downward sloping, as is expected when an incoherent scattering element (e.g. hydrogen) is present in the material. The signal to noise ratio was calculated for three peaks in each pattern. The peaks were selected to represent low, medium, and high Q. The signal was taken as the highest intensity point from the given peak and the noise was calculated by taking the average counts for 11 points from the area highlighted with a red square.

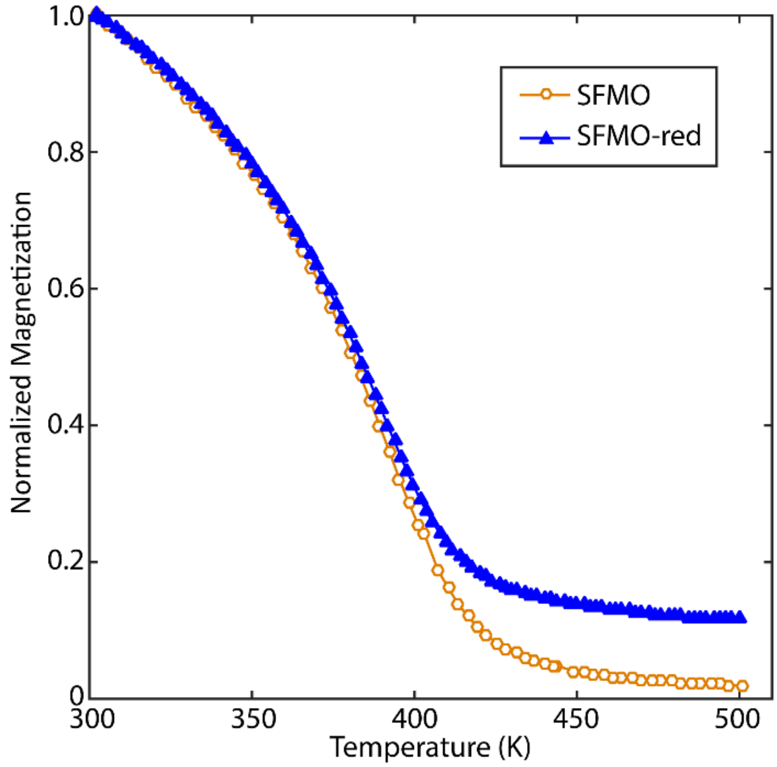

Figure S5. Magnetization versus temperature (cooling) for the starting material, Sr_2FeMoO_6 (SFMO), and the reduced material, Sr_2FeMoO_{6-x} (SFMO-red) under an applied field of 0.5 Tesla. Magnetization data is normalized to its value at 300 K.

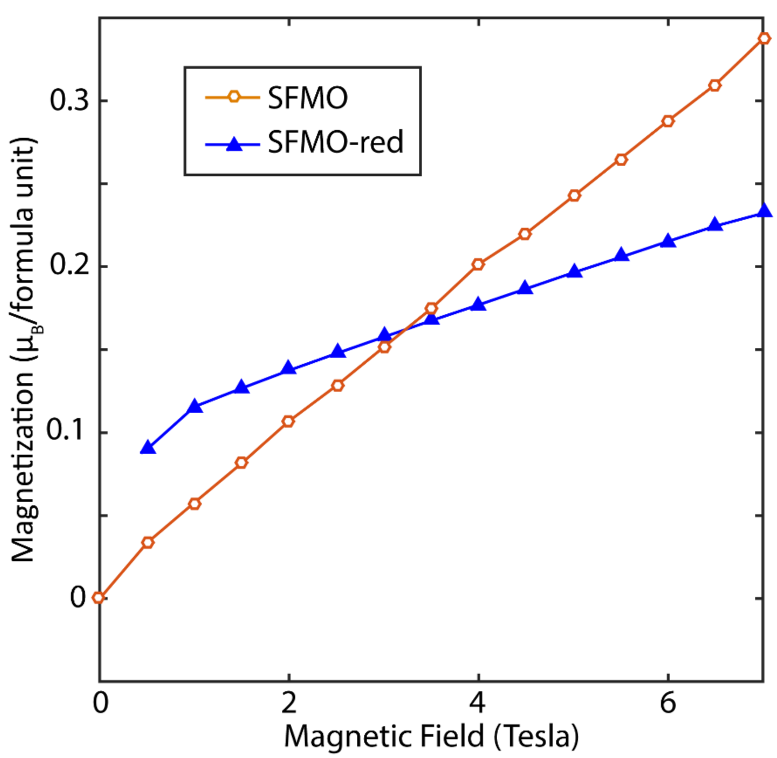

Figure S6. Magnetization versus field at 500 K (paramagnetic region) for the starting material, Sr_2FeMoO_6 (SFMO), and the reduced material, Sr_2FeMoO_{6-x} (SFMO-red).

Table S1. Complete refinement parameters for synchrotron X-ray and neutron powder diffraction experiments. ASD is the percent disorder on the B-site sublattice and rot. angle is the octahedral tilt angle.

		Sr_2FeMoO_6			Sr_2FeMoO_{6-x}	
Temperature		300 K		500 K	300 K	500 K
Technique		S-XRD		NPD	S-XRD	NPD
Space Group		*I*4/*m*		*Fm*-3*m*	*Fm*-3*m*	*Fm*-3*m*
a (Å)		5.572022(7)		7.90784(6)	7.890986(7)	7.90795(6)
c (Å)		7.90426(1)		-	-	-
volume ($Å^3$)		245.4069(7)		494.51(1)	491.353(1)	494.53(1)
ASD%		10.5(2)		-	14.0(2)	-
rot. angle (°)		7.93		0	0	0
Sr	(0 1/2 1/4)		(1/4 1/4 1/4)			
	B_{iso}	0.689(6)	B_{iso}	1.16(2)	0.720(6)	1.13(2)
Fe	(0 0 1/2)		(0 0 0)			
	B_{iso}	0.25(1)	B_{iso}	0.49(4)	0.43(1)	0.50(5)
Mo	(0 0 0)		(1/2 1/2 1/2)			
	B_{iso}	0.356(7)	B_{iso}	0.66(5)	0.256(6)	0.66(6)
O(1)	(*x* *y* 0)		(*x* 0 0)			
	x	0.2284(6)	*x*	0.2533(4)	0.2543(2)	0.2530(5)
	y	0.2630(4)				
	occ	1.006(3)	*occ*	1.000(5)	0.929(3)	0.898(4)
	B_{iso}	1.08(4)	U_{11}	0.0070(5)	-	0.0061(5)
			U_{22} & U_{33}	0.0241(3)	-	0.0232(3)
			(U_{12} & U_{13} & U_{23} = 0)			
			B_{iso}	-	1.01(2)	-
O(2)	(0 0 *z*)					
	z	0.2456(3)				
	occ	1.006(3)				
	B_{iso}	0.86(4)				
R_{wp}		10.09		7.33	8.38	4.72
χ^2		1.69		1.13	1.5	1.14